PHYSICAL REVIEW B **82**, 014112 (2010)

Oxygen/noble gas binary phase diagrams at 296 K and high pressures

Gunnar Weck, Agnès Dewaele, and Paul Loubeyre
CEA, DAM, DIF, F-91297 Arpajon, France
(Received 17 May 2010; published 28 July 2010)

The binary phase diagrams of O_2/rare gas (He, Ne, Ar, and Xe) mixtures have been measured at 296 K up to 20 GPa in a diamond-anvil cell. The boundary lines were determined by visual observation and by the Raman frequency of the O_2 vibron mode. The O_2-He phase diagram is of eutectic type with a liquid-liquid miscibility gap and complete immiscibility in the solid phase. The O_2-Ne phase diagram is of eutectic type with partial immiscibility in the solid phase. The O_2-Ar phase diagram is of azeotrope type and three different structures of Ar/O_2 solid solutions have been identified. The O_2-Xe phase diagram is of peritectic with eutectic type. The stoichiometric compound $Xe(O_2)_2$ is observed and characterized as a laves phase with a cubic structure isomorphous to $MgCu_2$. A qualitative understanding of these various diagrams is reached by the comparison of the effective hard-sphere diameters of the various species in the 10 GPa range. Some of the usefulness of the knowledge of these binary phase diagrams is highlighted: as a reference data set to test theoretical calculations on mixtures; to grow single crystal of O_2 in a rare-gas pressure medium; and to synthesize rare-gas oxides at high pressure.

DOI: 10.1103/PhysRevB.82.014112 PACS number(s): 62.50.−p, 64.70.kt, 64.75.Nx

I. INTRODUCTION

We present here an extensive high-pressure study of the binary phase diagrams of O_2 with rare gases (He, Ne, Ar, and Xe) at 296 K. Up to now, the study of the thermodynamical and structural properties of the mixtures of O_2 with rare gases has been limited essentially to $Ar_xO_{2(1-x)}$ systems at ambient pressure and low temperature.[1] In particular, many authors have contributed to the understanding of the properties of the Ar/O_2 cryosolid solutions that exist over the entire concentration range.[2–4] The essential issues discussed have been the structural changes in the end-component solids, Ar or O_2, under the gradual dissolution of the other components. Turning on the pressure parameter for the study of molecular binary mixtures reveals a rich class of new phenomena, such as a possible stability of stoichiometric compounds or an increase influence of the pressure-induced chemical changes in the species. Specifically addressed in the present study: does a van der Waals compounds exist in any mixture of O_2 with a rare gas, as observed for H_2, with $Ar(H_2)_2$ (Ref. 5) and $Xe(H_2)_7$ (Ref. 6), and N_2, with $He(N_2)_{11}$ (Ref. 7)? How does the molecular association of O_2 into O_8, observed above 10 GPa in the solid phase,[8,9] influence the binary phase diagrams of O_2 with rare gases? It is still formidably challenging to address these issues theoretically. Hence, the present measurements should constitute a reference data set to test improved theoretical methods for computing dense molecular alloys.[10] The present study was also motivated by two applications. First, the search for a topology of phase separation which could give a single crystal of O_2 embedded in a rare-gas pressure medium. Second, the search for stable O_2/Xe alloys that could favor the synthesis of xenon oxide at high pressure from a topochemical principle. The outline of the paper is the following: in Sec. II, experimental details are presented; the binary phase diagram of O_2 with He, Ne, Ar, and Xe are constructed in Sec. III; and the x-ray measurements of the three structures of the Ar-O_2 solid solutions and of the $Xe(O_2)_2$ van der Waals compounds are presented in Sec. IV; Interpretations and usefulness of this data set are discussed in Sec. V.

II. EXPERIMENTS

The binary phase diagram is the locus of boundary surfaces in the three-dimensional thermodynamical space, pressure (P), temperature (T), and the O_2 molar concentration (X). In the present study, the temperature is fixed at 296 K. The boundary lines in the (P,X) diagram have been investigated by measuring changes in the properties of the sample by varying pressure. A membrane diamond-anvil cell has been used, allowing very controlled and smooth variations in pressure, with a sensitivity of 0.02 GPa. The pressure range of the present study is 0.2–20 GPa. The membrane diamond-anvil cell equipped with 500 μm flat culet anvils was loaded at room temperature in a high-pressure vessel, typically under a pressure of 20 MPa to avoid the use of a compressor. Mixtures were directly made in the pressure vessel. The initial concentration of the mixture was fixed from the partial pressures of the gases, corrected with the virial coefficients. The loading of the diamond anvil cell was done after sufficient time for homogenization (12 h). The error bar on the concentration is less than 1 mol %. Inox 301 or rhenium gaskets were used. The sample chamber was typically around 80 μm in diameter at 10 GPa. The pressure was measured with the ruby luminescence technique using the quasihydrostatic ruby scale.[11] The error bar in pressure is ± 0.05 GPa. Depending on the system, 7–20 different initial concentrations have been studied and measurements at some concentrations have been repeated to test reproducibility.

Three different kinds of measurements have been performed to probe phase transitions in a given mixture under pressure. Phase boundaries have been clearly detected by visual observation through a microscope apparatus associated with the pressure measurement. The sample was observed at each point from a few minutes (in helium-oxygen

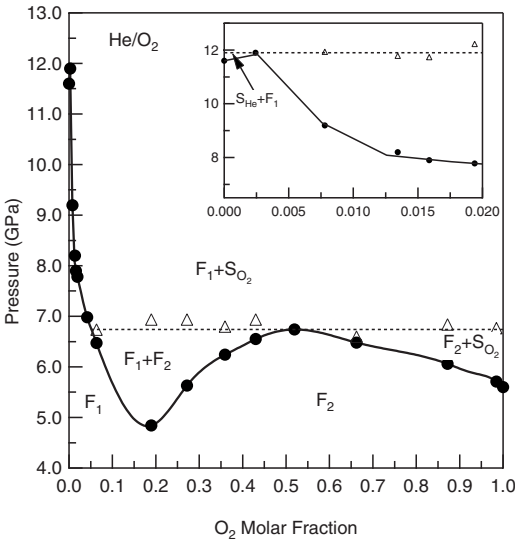

FIG. 1. Experimental binary phase diagram of the $He-O_2$ system. The black circles are experimental points of the liquidus. Triangles correspond to the pressure of the triple points measured for different concentrations. The inset corresponds to a zoom around the second triple point at 11.9 GPa and 0.25%.

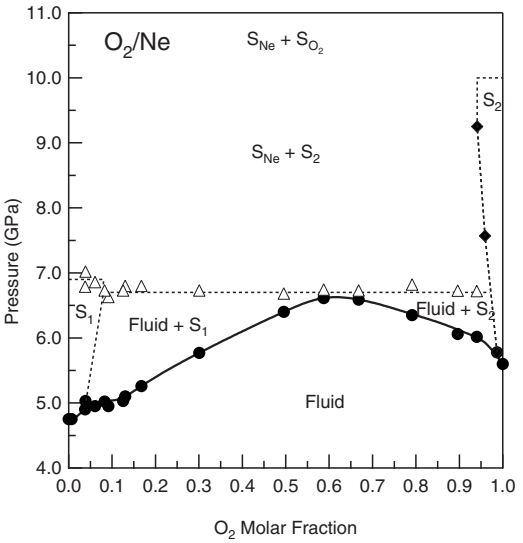

FIG. 2. Experimental binary phase diagram of the $Ne-O_2$ system. Black circles are experimental points of the liquidus. Triangles correspond to the pressure of the triple point measured for each concentration. Black diamonds correspond to the neon solubility in solid S_2 measured by x-ray diffraction.

or neon-oxygen mixtures) to several hours (in xenon-oxygen mixtures) to test for equilibration. Solid-fluid equilibrium could easily be observed. The transition points were the most finely detected by working with a single crystal in equilibrium with a fluid. The liquidus line was then delimited by the locus of the $P(X)$ points where the single crystal was seen to disappear. The solidus line corresponds to the locus of $P(X)$ points where the single crystal is seen to fill the whole sample chamber. Solid-solid transitions could be detected visually as well. Raman spectroscopy of the vibron mode of O_2 has been used to quantify the solubility of O_2 in the rare-gas matrix, to precisely confirm the phase transitions by looking at discontinuities of the vibron frequency with pressure, to determine the number of sites in O_2-Ar solid solutions (usually associated with different vibron frequencies), and to prove the existence of the $Xe(O_2)_2$ compound. Finally, the structures of the O_2/rare gas alloys have been determined by x-ray diffraction at the ESRF using angle dispersive monochromatic x-ray diffraction at 0.3738 Å (on ID30 or ID27) and at 0.3304 and 0.4180 Å (on ID09). The diffracted signal has been recorded on a MAR345 image plate.

III. BINARY PHASE DIAGRAMS

A. Helium-oxygen mixtures

The $He-O_2$ binary phase diagram has been determined mainly by visual observation. Sixteen different concentrations have been investigated at 296 K. The binary phase diagram is plotted in Fig. 1. The phase diagram is of eutectic type with a liquid-liquid miscibility gap. It has two triple points: one corresponding to an equilibrium $F_1+F_2+S_{O_2}$ at 6.7 GPa and 52 mol % O_2 and the other one corresponding to the equilibrium $S_{He}+F_1+S_{O_2}$ at 11.9 GPa and 0.25 mol % O_2. The inset of Fig. 1 shows more finely the measurements around the second triple point. Complete immiscibility in the solid phase is observed. Above 11.9 GPa, at any concentration, a solid-solid phase separation is observed. One phase is pure solid helium and the other is pure solid oxygen. From the volume of solid O_2 phase separated from solid helium at the concentration 0.25 mol % O_2 and from the absence of Raman O_2 vibron signal in solid helium, we estimated that the solubility of O_2 in solid helium should be less than 0.01 mol % O_2. For the 98.5 mol % O_2 mixture, a solid-solid phase separation has been observed. From the ratio between the volumes of the two solid phases in equilibrium, the solubility of He in solid oxygen is estimated to be smaller than 1 mol % O_2. X-ray diffraction measurements on a single crystal of O_2 grown in helium have shown no effect of a possible residual solubility of He in solid O_2 on the equation of state nor on the structural changes. Finally, since O_2 and N_2 systems under pressure have very similar intermolecular interactions, the existence of a van der Waals compound, similar to the observed $(N_2)_{11}He$,[7] was seen to be probable. The reason for the absence of a similar compound in O_2-He mixture is probably due to the exchange term in the interaction between O_2 molecules.

B. Neon-oxygen mixtures

The $Ne-O_2$ binary phase diagram has been determined at room temperature, mainly by visual observation. Seventeen different initial concentrations have been studied. Raman spectroscopy measurements and x-ray diffraction experiments were performed to characterize the solid phases. The $Ne-O_2$ binary diagram is plotted in Fig. 2. It is of eutectic type with partial immiscibility in the solid phase below 10 GPa and complete immiscibility above. The eutectic point is at 6.7 GPa and 62.5 mol % O_2. There is a small oxygen miscibility (4 mol % O_2) below 6.7 GPa in the neon-rich

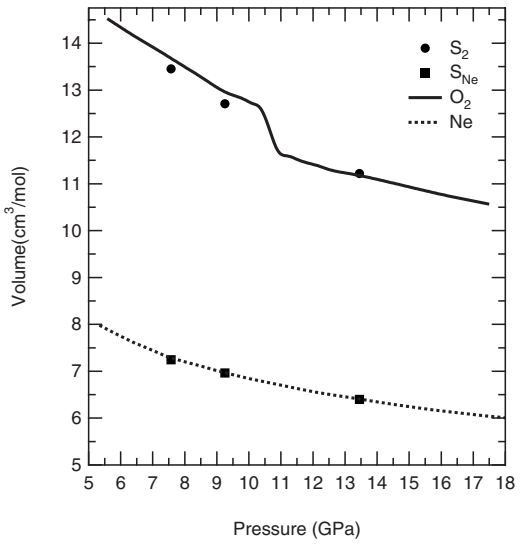

FIG. 3. Isothermal (296 K) equation of state of S_{Ne} and S_2. The equations of state of pure neon (Ref. 12) and pure oxygen (Refs. 8, 13, and 14) are plotted as reference.

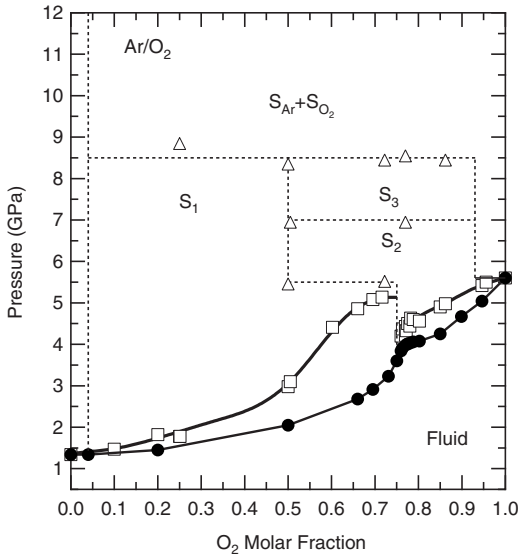

FIG. 4. Experimental binary phase diagram of the Ar-O_2 system. Black circles and open squares are experimental points of, respectively, the liquidus and the solidus lines. Open triangles and dashed lines indicate the stability limits of the S_1 (hcp), S_2 (*Pm*3*n*), and S_3 (*I*-42*d*) solid solutions. Below 5 mol % O_2, the solid has the fcc structure of argon.

solid (S_1). Above this pressure, an oxygen release from solid S_1 is observed and the solubility of O_2 is estimated to fall below 1 mol % O_2. From visual observation, the solubility of neon in oxygen-rich solid (S_2) has been estimated to be smaller than 6 mol %. But, it was not possible to follow the change in this solubility either from visual observation or Raman measurement (no measurable Raman O_2 vibron frequency shift is associated with this Ne solubility).

X-ray diffraction measurements have been performed on the S_1+S_2 phase separation obtained in an O_2/Ne mixture of 53 mol % O_2 initial concentration. The sequence of phase transitions observed in S_2 is identical to pure solid O_2, namely (β-O_2,$R\bar{3}m$), above 9.3 GPa (δ-O_2,*Fmmm*) and above 13.5 GPa (ε-O_2,$C2/m$[13]). The volume of S_1 and S_2 is compared in Fig. 3 to the equation of state of pure solid Ne and pure solid O_2. The S_1 solid has the same face-centered-cubic (fcc) structure and the same molar volume as pure solid neon which confirms the visual observations of a complete immiscibility of oxygen in solid neon above 7 GPa. The volume of S_2 is seen to be smaller than the one of pure solid O_2. Under ideal mixing assumption, the molar concentration of Ne in S_2 is estimated to be 5 mol %. Above 8.5 GPa, the molar volume of S_2 falls on the equation of state of O_2, implying that the solubility of Ne in S_2 drops below 1 mol %.

C. Argon-oxygen mixtures

The Ar-O_2 binary phase diagram has been measured at 296 K, mainly by visual observation. A total of 40 samples have been prepared to cover finely the whole concentration range. The Ar-O_2 binary phase diagram is plotted in Fig. 4. It is of the azeotrope type, with a congruent melting at 75 mol % O_2. For oxygen concentrations above 93% there is a solid-solid phase separation above 5.6 GPa. The solidus line has a strong discontinuity at 75 mol % O_2, indicative of a structural change in Ar/O_2 alloys at this concentration. Above 9.5 GPa, the alloys completely phase separate into almost pure fcc Ar and ε-O_2, identified by x-ray diffraction. For O_2 concentrations smaller than 5 mol %, no phase separation is observed; the amount of O_2 dissolved in solid Ar above 9.5 GPa is thus estimated to be around 5 mol % O_2. From Raman measurements of the O_2 vibron, three Ar/O_2 alloys—S_1, S_2, and S_3—have been identified. Their boundary lines are plotted in Fig. 4. Raman frequencies measured in these alloys are reported in Fig. 5. In S_1, only one vibron peak is observed; in addition, x-ray diffraction measurements showed that S_1 has the hcp structure. In S_2 and S_3, two vibron peaks are measured, which have a 1.5 intensity ratio independent of the O_2 concentration. This implies that S_2 and S_3 are solid solutions of Ar and O_2 with random distribution on the sites and that they have a structure with two different sites at least. From x-ray diffraction data, the S_2 structure is identified as *Pm*3*n*. The S_3 structure has not been fully resolved but is probably a tetragonal distortion of the S_2 with possible space group *I*-42*d*. Both structures allow the random substitution of O_2 molecules by Ar atoms on the γ-O_2 structure. It is very similar to what has been obtained for Ar-O_2 cryosolid solutions.[4] The gamma phase of oxygen is quite stable to the dissolution of argon in it, up to 50 mol % Ar. Above 7 GPa the symmetry is reduced and a doubling of the cell obtained. That is described in more detail in Sec. IV.

D. Xenon-oxygen mixtures

Seven Xe-O_2 samples with various initial concentrations have been studied at 296 K. The liquidus line has been determined by visual observation. The stability domains in the solid phase have been determined by the combination of visual observation, Raman spectroscopy and x-ray diffraction.

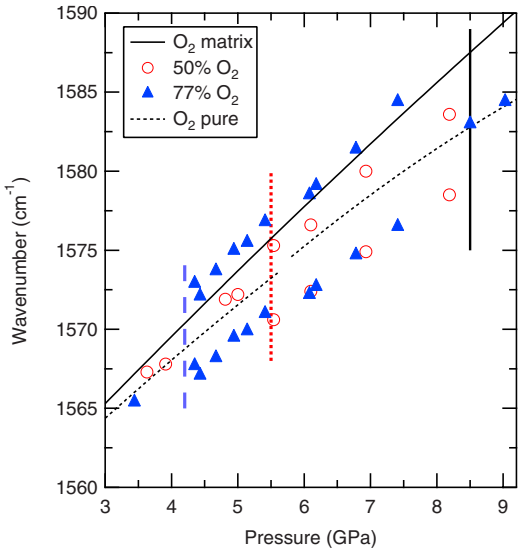

FIG. 5. (Color online) Oxygen vibron frequency measured for different concentrations of Ar-O_2 mixtures. The vertical dashed line corresponds to the fluid-S_2 transition observed at 77 mol % O_2. The vertical dotted line represents the S_1-S_2 transition observed at 50 mol % O_2. The vertical straight line corresponds to the phase separation observed above 8.5 GPa in S_1 and S_3.

The Xe-O_2 binary phase diagram is plotted in Fig. 6. It is of peritectic with eutectic type. The eutectic point is at 5.95 GPa and approximately 98 mol % O_2 and the peritectic point around 75 mol % O_2 at 3.1 GPa. The presence of a peritectic point reveals the stability of a Xe/O_2 compound. The O_2 vibron frequencies versus pressure, for various initial concentrations, are plotted in Fig. 7. This indicates the existence of three stable solid phases in Xe/O_2 mixtures: a solid rich in Xe, S_1, a stoichiometric compound and pure oxygen. Both S_1 and the compound have only one O_2 vibron Raman

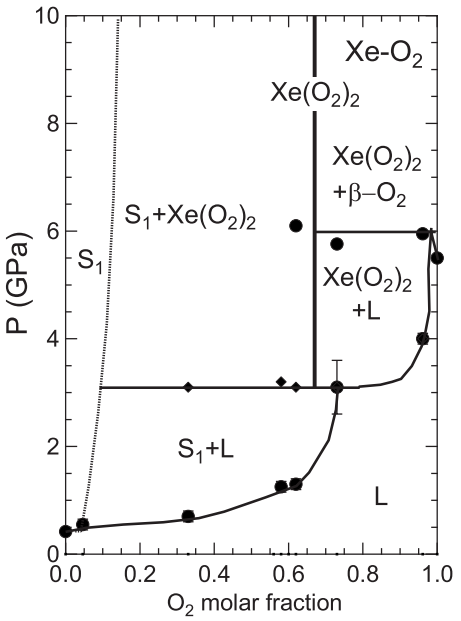

FIG. 6. Binary phase diagram of the Xe-O_2 system. Black symbols represent experimental points and lines interpolations between these points.

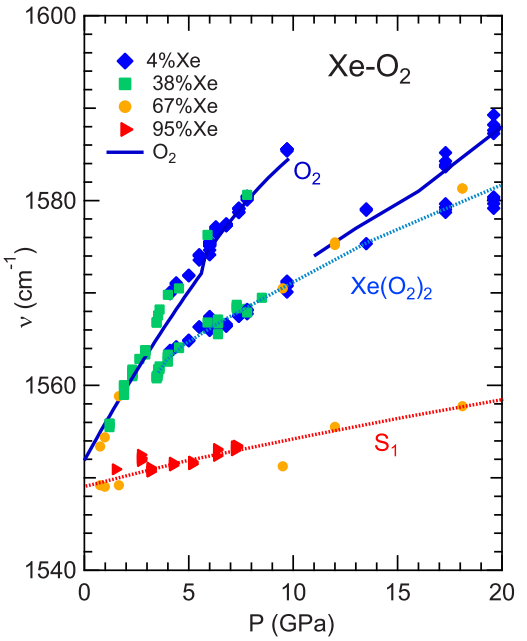

FIG. 7. (Color online) Evolution of the frequencies of the intramolecular O_2 vibron with pressure measured for different concentrations of Xe-O_2 mixtures. The frequencies measured in S_1 and $Xe(O_2)_2$ are lower than the frequency in pure O_2 (Ref. 15).

frequency, lower than the one measured in pure oxygen. The solubility of Xe in solid O_2 is estimated to be lower than 1 mol % from the lever rule applied to the volumes of the two solid phases separated in the mixture of initial concentration 96 mol % O_2. The solubility of O_2 in solid Xe was seen to increase with pressure, starting from about 1 mol % O_2 at the solidification pressure of Xe, 0.42 GPa, to approximately 15 mol % O_2 above 4 GPa. This leads to a gradient of concentration in solid S_1. X-ray diffraction shows that the structure of S_1 is fcc as pure solid Xe. The fcc structure of Xe is thus remarkably stable upon the dissolution of up to 15 mol % O_2 in it up 10 GPa. As presented in more detail in the next paragraph, the x-ray study of the stoichiometric compound was used to determine its exact formula. We found that it is $Xe(O_2)_2$, with the $MgCu_2$-type Laves phase structure.[16] It is assumed that the O_2 and Xe entities occupy, respectively, the Cu and Mg sites. The fact that only one site is occupied by O_2 molecule matches the observation of only one Raman vibron mode, as reported in Fig. 7.

IV. STRUCTURAL DETERMINATION OF ArO_2 AND $Ar(O_2)_3$ ALLOYS AND $Xe(O_2)_2$ VAN DER WAALS COMPOUND

The three different structures of Ar/O_2 solid solutions have been characterized by x-ray diffraction under pressure of three mixtures of different initial concentrations. At 25 mol % O_2 and 50 mol % O_2, the mixture solidifies into the S_1 phase and easily forms a single crystal. The observed diffraction peaks could be indexed and correlated with a hexagonal unit cell with two molecular entities in it (space group $P63/mmc$). In the 75 mol % O_2 mixture, a single crystal S_2 is grown from the melt. The diffraction peaks could be in-

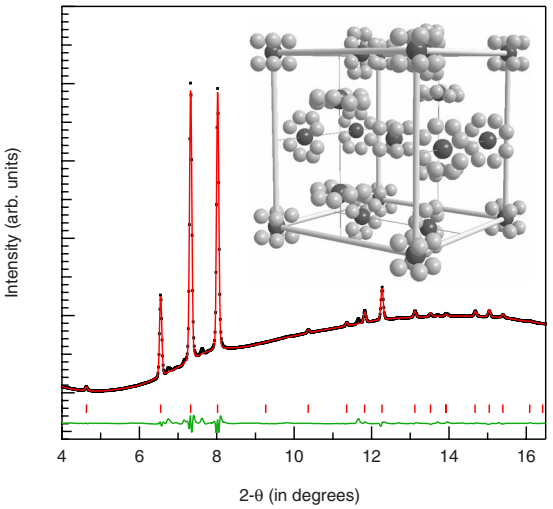

FIG. 8. (Color online) X-ray diffraction pattern collected in a mixture of 50 mol % Ar-50 mol % O_2 at 6.9 GPa. The dots correspond to the measured pattern and the line to the calculated pattern after a Rietveld refinement. The inset shows a schematic view of the S_2 crystal with argon and oxygen atoms, respectively, in dark and light gray.

dexed and correlated with a cubic $Pm3n$ space group with eight molecular entities in the unit cell. The structure is thus very similar to the gamma phase of cryo-Ar-O_2 solid solutions.[4] From Raman measurements showing that the intensity ratio between the two oxygen vibrons is independent of concentration, we assume that there is a random substitution of O_2 by Ar on the ($2a$) and ($6c$) sites of the gamma phase of oxygen.[17] Yet, we cannot completely rule out the existence of a preferential substitution. That would require a full refinement of the atomic positions using single-crystal x-ray diffraction data. In the 50 mol % O_2 mixture, the S_1 transforms into the S_2 phase at 5.5 GPa. The transition breaks the single crystal. A powder pattern of the S_2 phase obtained in the 50 mol % O_2 mixture at 6.9 GPa is presented in Fig. 8. The data are well indexed using $Pm3n$ space group with a=5.7828 Å. The Rietveld analysis program GSAS (Ref. 18) was used for the structure refinement. The structural parameters are presented in Table I.

Finally the S_2 phase transforms into the S_3 phase at 7 GPa. This transition, observed by x-ray diffraction in the 50 and 75 mol % O_2 mixture, is expected to occur regardless of the concentration in S_2. The powder patterns of S_3 obtained in the 50 mol % O_2 mixture at 7.5 GPa is presented in Fig.

TABLE I. Refined structural parameters of the S_2 crystal (space group $Pm3n$) for a 50 mol % O_2 structure at 6.9 GPa and 296 K.

Unit cell a_{cub}=5.7828 Å				
Label	x	y	z	Occ
A_R1	0.0000	0.0000	0.0000	0.500
O1	0.05988	0.05988	0.05988	0.125
A_R2	0.2500	0.5000	0.0000	0.500
O2	0.2367	0.4869	0.1020	0.125

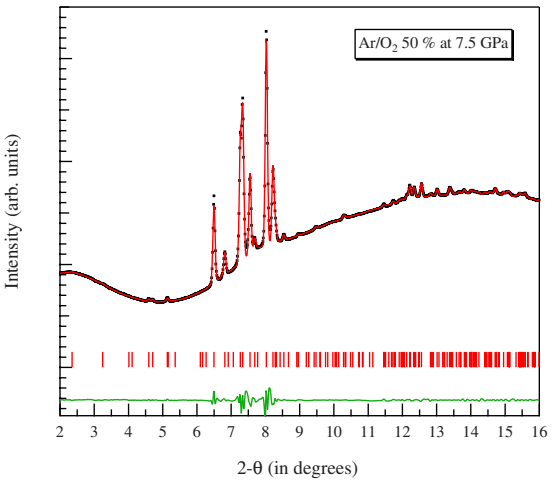

FIG. 9. (Color online) X-ray diffraction pattern collected in a mixture of 50 mol % Ar-50 mol % O_2 at 7.5 GPa (top). The dots correspond to the measured pattern and the line to the calculated pattern after a Lebail refinement.

9. The diffraction pattern indicates a tetragonal distortion of the cubic phase. The situation is thus similar to what has been observed in pure solid nitrogen at the δ-δ^* phase transition[19] but the $P4_2/ncm$ space group proposed for δ^* does not fit all the diffraction lines. The present diffraction pattern is correctly indexed by a tetragonal unit cell with the lattice parameters a=11.6606 Å and c=11.1970 Å. This corresponds to a doubling of the lattice parameters of the gamma phase as already reported at low temperature.[4] Therefore, the structure of S_3 is assumed to be an analog of the structure of the low-temperature δ phase of Ar-O_2 solutions (symmetry group I-43d) with possible space group I-42d. The Rietveld refinement of the data to determine the exact atomic positions was unsuccessful.

The diffraction pattern of the $Xe(O_2)_2$ compound has been collected on a polycrystalline solid in equilibrium with a O_2-rich fluid at 3.7 GPa, in a mixture of 75 mol % O_2 concentration. The integrated diffraction pattern is presented in Fig. 10. The pattern can be best indexed by an $Fd3m$ cubic unit cell. The volume of the unit cell almost matches $8 \times V_{Xe} + 16 \times V_{O_2}$ at the same pressure.[20,21] We propose that the $Xe(O_2)_2$ adopts the $MgCu_2$-type Laves phase structure,[16] with O_2 and Xe occupying, respectively, the Cu and Mg sites. As discussed in the next section, based on the molecular size ratio, an AB_2 Laves phase was expected in the Xe/O_2 mixture, as observed for $Ne(He)_2$ (Ref. 22) and $Ar(H_2)_2$.[5] The $Xe(O_2)_2$ compound has been drawn in Fig. 10. The orientation of the molecules could not be refined by a Rietveld refinement of the powder spectra because of the too small number of crystallites in the x-ray beam. The orientation of the O_2 molecules has been drawn to optimize a quadrupolar order, as in ε-N_2.[23] At higher pressure, the volume of $Xe(O_2)_2$ remains close to the ideal mixing value of as shown in Fig. 11.

V. DISCUSSION

An important conclusion from studies on metallic alloys is that the solid-state solubility is governed mainly by geo-

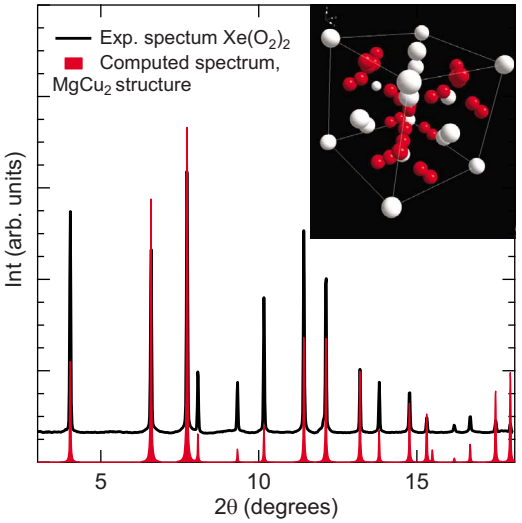

FIG. 10. (Color online) X-ray diffraction pattern obtained in a mixture of 25 mol % Xe-75 mol % O_2 at 3.7 GPa and 296 K. A picture of the bidimensional pattern is presented together with the circularly integrated pattern. It is compared with a theoretical diffraction pattern for a $Xe(O_2)_2$ solid with the $MgCu_2$ Laves phase structure and a lattice parameter of 9.20 Å [space group $Fd3m$ (Ref. 16)]. The sample chamber is filled with numerous crystals of $Xe(O_2)_2$, in equilibrium with a O_2-rich fluid. Inset: picture of $Xe(O_2)_2$ with the $MgCu_2$ structure. Xenon atoms and oxygen molecules are, respectively, drawn in white and red.

metrical effects, as expressed by the well-known Hume-Rothery rule.[25] This rule was shown to explain the shape of the phase diagrams of helium with other rare gases under pressure. This empirical rule applied here would state that solid solutions should exist if the effective molecular diameter of the two species do not differ by more than 15%. The effective diameter of a molecular species at a given pressure

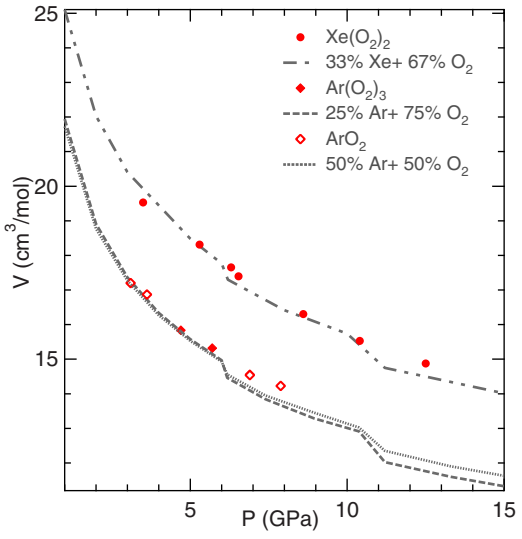

FIG. 11. (Color online) Isothermal (296 K) equations of state of $Xe(O_2)_2$ compound, ArO_2 and $Ar(O_2)_3$ alloys. The compression curves for ideal solutions of 33% Xe-67% O_2, 50% Ar-50% O_2, and 25% Ar-75% O_2, as calculated from the EOS of pure O_2 (Refs. 13, 14, and 20), pure Ar (Ref. 21), and pure Xe (Ref. 24), are also plotted.

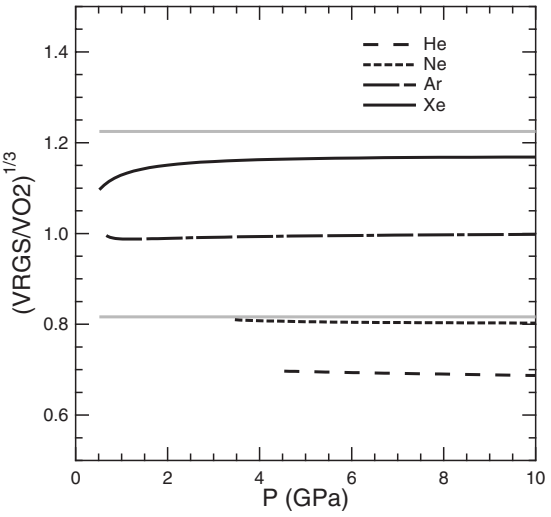

FIG. 12. Evolution of atomic/molecular radii ratios with pressure for the studied rare gases and oxygen (Refs. 12–14, 20, 21, 24, and 26). The ideal ratios for Laves phases with compositions $RGS(O_2)_2$ and $O_2(RGS)_2$ (respectively, 1.225 and 0.816) are represented as continuous gray lines.

is proportional to the cubic root of its molar volume. The ratio of the rare-gas effective diameter over that of O_2 versus pressure is plotted in Fig. 12. The ratio is almost unity for Ar/O_2 so a large concentration range of solid solutions is expected, as observed. For all the other rare gases, the difference is larger than 15%: slightly larger than 15% for Xe, explaining the partial miscibility—up to 15 mol % O_2 in solid Xe; about 20% difference for Ne, explaining the small miscibility of Ne in O_2 and vice versa and more than 30% difference for He, explaining the complete immiscibility in the solid phase. Furthermore, for a large difference, a fluid-fluid miscibility gap is expected, as observed in the He/O_2 case.

In addition to substitutional alloys, various stoichiometric compounds can be formed. For hard-sphere systems, several types of stoichiometric compounds have been proposed, which optimize packing. By increasing small to large hard-sphere diameter ratios α, compounds of type AB ($\alpha \leq 0.4$), AB_2 ($\alpha \simeq 0.5$), and AB_{13} ($\alpha \simeq 0.6$) have been predicted.[27] However none of these compounds have been observed so far in molecular mixtures under pressure. For $\alpha \simeq 0.8$, a class of AB_2 compounds are expected,[28] usually referred to as Laves phases. These phases have been first observed in metallic binary systems; the most efficient packing is obtained for $\alpha = 0.816$. The Laves phases crystallize in one of the three closely related structures,[16] isomorphous with the compound $MgCu_2$ (cubic cell, 8 f.u.), $MgZn_2$ (hexagonal cell, 4 f.u.), or $MgNi_2$ (hexagonal cell, 8 f.u.). As seen in Fig. 12, the effective diameter of O_2 is 0.84 times that of Xe, close to the ideal value of 0.816 and indeed a $Xe(O_2)_2$ compound is observed. On the other hand, the effective diameter of Ne is 0.8 times that of O_2 but the compound $O_2(Ne)_2$ has not been observed. Hence, consideration of efficient packing is certainly not the only parameter explaining the formation of Laves phases in molecular systems. As it was shown previously on the $Ne(He)_2$ case, the formation of the Laves phase is driven by both entropy and energy.[29] An elaborate Gibbs energy calcu-

lation to fully explain the stability of the $Xe(O_2)_2$ compound is beyond the scope of the present work.

Ne, Ar, and Xe rare-gas solids have a fcc structure. At least up to 200 GPa for Ne (Ref. 12) and Ar (Ref. 21) whereas a sluggish transition from fcc to hcp is observed in Xe over the pressure range 14 GPa–75 GPa.[30] It is well known that the dissolution of small impurities in cryorare-gas solids tend to favor the hcp structure. For example, the dissolution of no more than 1% O_2 in fcc cryo-Ar stabilizes the hcp structure.[31] It was thus expected that the fcc structure would be destabilized by the addition of oxygen. It is observed here that the fcc structure is more resistant to the dissolution of O_2 at high pressure since up to 5 mol % O_2 can be mixed with fcc Ar and fcc Ne before the solid solution adopts the hcp structure. More surprisingly, Xe-O_2 solid solutions with up to 15 mol % O_2 retain the fcc structure. The fact that the rare gas with the least stable fcc structure under pressure is the one that can dissolve the larger amount of O_2 without changing to the hcp structure is thus counterintuitive and should motivate detailed calculations.

The dramatic change in Ar/O_2 mixtures from full miscibility above the solidus line to complete immiscibility above 9 GPa is striking. The Hume-Rothery rule is highly violated here. The explanation originates from the sharp phase transition that occurs in pure solid O_2 above 10 GPa. The nature of this phase transition has been recently elucidated as the molecular association of 4 O_2 molecules into a rhombohedral $(O_2)_4$ unit.[8,9] The presence of this new chemical bond between O_2 molecules affects the miscibility in the O_2/Ar mixture. That also explains the opening of the miscibility gap in Ne/O_2 mixtures above 9 GPa. This implies that the computation of the Ar/O_2 binary phase diagram above 10 GPa would have to be treated at the *ab initio* level. That is still a formidable challenge.

We have selected here below some applications of the present determination of the O_2/rare gas binary phase diagrams, one for each diagram: (1) the growth of O_2 single crystals in a helium pressure medium.[8,14] At 10 GPa, i.e., at the δ-ε transition, solid oxygen undergoes significant changes in its properties. The ε phase remains stable up to 96 GPa, above which the solid becomes metallic (ζ phase). The structures of the ε and ζ phases remained unsolved for decades, partly because of the low quality of the diffraction patterns obtained with pure oxygen powders. By exploiting the topology of the complete solid immiscibility in O_2/He mixtures, very good quality ε single crystals could be grown in helium. Practically, the crystal is grown in a O_2/He mixture with an initial 2.5 mol % O_2 concentration and occupies one third of the full sample thicknesses at 20 GPa. But, at this concentration, the phase separation appears at 8 GPa at room temperature, i.e., below the β-δ-ε sequence of transition. To directly phase separate in the stability domain of the ε phase, the single crystals were slowly grown at 450 K and 22.5 GPa.

(2) Formation of fine O_2 powder in Ne.[14] In O_2/Ne mixtures, by rapidly increasing pressure from the fluid phase, a mixed powder of O_2 and Ne crystals is obtained, with grains less than 1 μm in diameter. Such a powder could be useful to perform Rietveld refinement in the metallic phase of solid oxygen and thus complement x-ray diffraction measurement on single crystal.

(3) Recrystallization from a fine-grained polycrystalline mixture of pure solid O_2 and solid Ar. The opening of a large miscibility gap in Ar/O_2 mixtures above 9 GPa transforms the $Ar(O_2)_3$ solid solution single crystal into a fine-grained polycrystalline mixture of Ar and O_2. Upon decreasing pressure below 9 GPa, a recrystallization of this powder into a single crystal of $Ar(O_2)_3$ is observed within few hours. That implies great mobility of atoms and molecules, unexpected when vacancy mechanisms are excluded. A more detailed analysis will be the subject of a future publication.

(4) Reactivity of Xe-O_2 mixture at high pressure. The topochemical principle implies that $Xe(O_2)_2$, where xenon atoms and oxygen molecules lie close to each other, is an ideal reactant to synthesize xenon oxides under high pressure.

VI. CONCLUSIONS

A series of O_2/rare gas binary phase diagrams at 296 K is presented here. The large range of differences in binary interactions explains the various types of binary phase diagrams observed, from an azeotrope type to an eutectic type with complete immiscibility in the solid phase and a liquid-liquid miscibility gap. Two salient results of the present work are the discovery of the $Xe(O_2)_2$ Laves phase compounds and the rich structural polymorphism in Ar/O_2 solid mixtures. A partial understanding of the various phase diagrams can be obtained, at a first level, from geometrical considerations. However, it is shown that this can be misleading at high pressure. The dramatic opening of an almost complete immiscibility gap in Ar/O_2 solid solutions above 9 GPa is understood by the chemical change in the O_2 molecules under pressure. That is the first observation of the effect of pressure-induced chemical changes on a binary phase diagram. *Ab initio* calculations seem to be the suited method for a microscopic investigation of the Ar/O_2 binary phase diagram. Yet remain a great challenge. Consequently, we believe that the present data set of O_2/rare gas mixtures should provide a useful corpus for testing calculations of mixture properties in molecular systems at high pressure. This is particularly important because there is a current great interest in the synthesis of new molecular materials by pressure. Part of the strategy for new molecular crystal engineering at high pressure is to control the ordering of the molecular entities in the reactant solid phase so as to preorganize the molecules in such a way to favor the reaction and the final product. Accurate predictions of the structural changes in binary mixtures will be an important step.

ACKNOWLEDGMENTS

The authors acknowledge the European Synchrotron Radiation Facility for provision of synchrotron-radiation facilities during beamtime allocated to proposal HS-4067. We are grateful to M. Mezouar on ID30/ID27 and to M. Hanfland on ID09 for experimental help.

[1] V. G. Manzhelii, A. I. Prokhvatilov, I. Y. Minchina, and L. D. Yantsevich, *Handbook of Binary Solutions of Cryocrystals* (Begell House, New York, 1996), Chaps. 2.6 and 3.4.
[2] A. Prokhvahtov and S. Barylnik, Sov. J. Low Temp. Phys. **11**, 707 (1985).
[3] T. Westerhoff and R. Feile, Phys. Rev. B **54**, 913 (1996).
[4] A. S. Baryl'Nik, A. I. Prokhvatilov, and A. I. Érenburg, Sov. J. Low Temp. Phys. **14**, 99 (1988).
[5] P. Loubeyre, R. Letoullec, and J. P. Pinceaux, Phys. Rev. Lett. **72**, 1360 (1994).
[6] M. Somayazulu, P. Dera, A. F. Goncharov, S. A. Gramsch, P. Liermann, W. Yang, Z. Liu, H. Mao, and R. J. Hemley, Nat. Chem. **2**, 50 (2010).
[7] W. L. Vos, L. W. Finger, R. J. Hemley, J. Z. Hu, H. K. Mao, and J. A. Schouten, Nature (London) **358**, 46 (1992).
[8] L. F. Lundegaard, G. Weck, M. I. McMahon, S. Desgreniers, and P. Loubeyre, Nature (London) **443**, 201 (2006).
[9] H. Fujihisa, Y. Akahama, H. Kawamura, Y. Ohishi, O. Shimomura, H. Yamawaki, M. Sakashita, Y. Gotoh, S. Takeya, and K. Honda, Phys. Rev. Lett. **97**, 085503 (2006).
[10] C. Cazorla, D. Errandonea, and E. Sola, Phys. Rev. B **80**, 064105 (2009).
[11] H. Mao, J. Xu, and P. Bell, J. Geophys. Res. **91**, 4673 (1986).
[12] A. Dewaele, F. Datchi, P. Loubeyre, and M. Mezouar, Phys. Rev. B **77**, 094106 (2008).
[13] B. Olinger and R. M. A. R. Roof, J. Chem. Phys. **81**, 5068 (1984).
[14] G. Weck, P. Loubeyre, and R. LeToullec, Phys. Rev. Lett. **88**, 035504 (2002).
[15] Y. Akahama and H. Kawamura, Chem. Phys. Lett. **400**, 326 (2004).
[16] R. Johnston and R. Hoffmann, Z. Anorg. Allg. Chem. **616**, 105 (1992).
[17] T. H. Jordan, W. E. Streib, H. W. Smith, and W. N. Lipscomb, Acta Crystallogr. **17**, 777 (1964).
[18] A. C. Larson and R. B. V. Dreele, Los Alamos National Laboratory, Technical Report No. LAUR 86-748, 2000 (unpublished).
[19] G. W. Stinton, I. Loa, L. F. Lundegaard, and M. I. McMahon, J. Chem. Phys. **131**, 104511 (2009).
[20] E. Abramson, L. Slutsky, M. Harrell, and J. Brown, J. Chem. Phys. **110**, 10493 (1999).
[21] M. Ross, H. K. Mao, P. M. Bell, and J. A. Xu, J. Chem. Phys. **85**, 1028 (1986).
[22] P. Loubeyre, M. Jean-Louis, R. LeToullec, and L. Charon-Gérard, Phys. Rev. Lett. **70**, 178 (1993).
[23] R. Mills, B. Olinger, and D. Cromer, J. Chem. Phys. **84**, 2837 (1986).
[24] A. Zisman, I. Aleksandrov, and S. Stishov, Phys. Rev. B **32**, 484 (1985).
[25] W. Hume-Rothery, G. W. Mabbott, and K. M. Channel Evans, Philos. Trans. R. Soc. London, Ser. A **233**, 1 (1934).
[26] A. Dewaele, J. Eggert, P. Loubeyre, and R. LeToullec, Phys. Rev. B **67**, 094112 (2003).
[27] X. Cottin and P. A. Monson, J. Chem. Phys. **102**, 3354 (1995).
[28] A.-P. Hynninen, J. H. J. Thijssen, E. C. M. Vermolen, M. Dijkstra, and A. V. Blaaderen, Nature Mater. **6**, 202 (2007).
[29] P. Loubeyre, High Press. Res. **14**, 353 (1996).
[30] A. P. Jephcoat, H.-k. Mao, L. W. Finger, D. E. Cox, R. J. Hemley, and C.-s. Zha, Phys. Rev. Lett. **59**, 2670 (1987).
[31] C. S. Barrett, L. Meyer, and J. Wasserman, J. Chem. Phys. **44**, 998 (1966).